Permeability and tomography-based microstructural analysis of ultra-porous bioactive glass scaffolds

Materials Letters 384 (2025) 138064

Contents lists available at ScienceDirect

Materials Letters

journal homepage: www.elsevier.com/locate/matlet

Permeability and tomography-based microstructural analysis of ultra-porous bioactive glass scaffolds

Alessandro Schiavi [a], Federico Gaido [b], Roberta Gabrieli [b], Dario Alidoost [a,c], Martin Schwentenwein [d], Mehdi Mohammadi [d], Dilshat Tulyaganov [e], Enrica Verné [b], Francesco Baino [b,*]

[a] National Institute of Metrological Research (INRiM) 10135 Turin, Italy
[b] Department of Applied Science and Technology, Politecnico di Torino 10129 Turin, Italy
[c] Interdepartmental Centre J-Tech, Politecnico di Torino 10129 Turin, Italy
[d] Lithoz GmbH 1060 Vienna, Austria
[e] Department of Natural-Mathematical Sciences, Turin Polytechnic University in Tashkent 100095 Tashkent, Uzbekistan

ARTICLE INFO

Keywords:
Bioactive glass
Porosity
Vat photopolymerization

ABSTRACT

Reliable and accurate quantification of permeability and microstructural characteristics of bioactive glass and ceramic scaffolds, which play a key role in dictating the mechanical and biological performance of the material, is challenging especially for highly-porous implants with intricate, delicate structures. In this study, we determine the major mass transport properties of exceptionally-porous bioactive glass scaffolds produced by vat photopolymerization through the implementation of the Ergun-Wu resistance model being properly supplied with experimental data. Specifically, Darcian intrinsic permeability determined via acoustic measurements and average pore diameter from the advanced micro-tomographic imaging of scaffolds were used as input to the model. An accurate and robust statistical analysis further confirms the soundness of the results obtained and of the overall methodological approach.

1. Introduction

Over the last years, permeability has been proposed as a "global" parameter to estimate scaffold suitability for potential application in bone tissue engineering [1]. Permeability depends on multiple parameters including the fraction and size of interconnected pores and pore tortuosity [2]; therefore, it is tightly related to mass transport properties that govern fluid penetration in the scaffold, dictate the rate of cell migration and vascularization, and ultimately affect bone in-growth and regeneration. However, the assessment of permeability in highly-porous solids with delicate internal structures, like bioceramic or glass scaffolds, still is a challenge.

Methods such as physical gas absorption, helium pycnometry or mercury intrusion porosimetry yield information about density, pore volume and pore size but do not provide a direct measurement of intrinsic permeability [3]. Ochoa et al. [4] experimentally assessed the permeability of 45S5 Bioglass® foams using deionized water, a peristaltic pump and by measuring the pressure drop across the scaffold. Other authors estimated permeability by computational approaches [5].

Our research group recently determined the intrinsic permeability of highly-porous (80 vol%) hydroxyapatite [6] or moderately-porous bioactive glass scaffolds (40 vol%) [7] by using an acoustic measurement system. In the present work, we pushed this approach to the limit for experimentally measuring the permeability and analytically calculating the microstructural properties of 3D-printed ultra-porous bioactive glass foams.

2. Materials and methods

2.1. Starting glass and scaffold production

The bioactive glass (BG-1d, composition 46.1SiO_2-28.7CaO-8.8MgO-6.2P_2O_5-5.7CaF_2-4.5Na_2O wt.%) used for making scaffolds was synthesized according to a melt-quenching route [8]. BG-1d was selected owing to its highly promising biological properties in vitro and in vivo [9]. Ultra-porous BG-1d cylindrical foams (total porosity 94 vol%) were

* Corresponding author.
E-mail address: francesco.baino@polito.it (F. Baino).

https://doi.org/10.1016/j.matlet.2025.138064
Received 1 October 2024; Received in revised form 8 December 2024; Accepted 13 January 2025
Available online 17 January 2025

produced by vat photopolymerization (Fig. 1); the process details and scaffold characterizations are reported in [10].

2.2. Model development

The analytical model to calculate the main microstructural parameters and mass transport properties of BG-1d scaffolds relies on the Ergun-Wu resistance model [11] applied for laminar oscillating flows in Darcy's regime [12]. The analytical model is based on the combination of Darcy's law and Forchheimer equation, as follows:

$$\left(-\frac{\partial p}{\partial x}\right) = \frac{\mu}{k}U = \mu a U + \rho b U^2 \tag{1}$$

where ∂p is the pressure loss gradient of the fluid flow (upstream and downstream) through the scaffold along the flow direction ∂x, U is the fluid velocity in the x-direction,k is the intrinsic permeability, μ is the dynamic viscosity of the fluid, ρ is the density of the fluid. The parameters a and b are expressed as a function of the pore morphology, as follows:

$$a = 72\tau\frac{(1-\varepsilon)^2}{\varepsilon^3}\bullet\frac{1}{D_{av}^2\varphi^2} \tag{2}$$

$$b = 0.75\tau\frac{(1-\varepsilon)}{\varepsilon^3}\bullet\frac{1}{D_{av}\varphi}\bullet\left(1.5-2.5\frac{1}{\beta^2}+\frac{1}{\beta^4}\right) \tag{3}$$

where τ is the pore tortuosity, ε is the effective porosity (i.e., the open porosity allowing the fluid to flow through the scaffold, without accounting dead-end pores and closed pores), D_{av} is the average pore diameter, φ is the pore shape factor (sphericity), and β is the pore narrowing ratio, which is related to the variation of pore cross-section. Pore tortuosity and narrowing ratio depend only on the effective porosity and can be calculated as $\tau = 1-0.4\ln(\varepsilon)$ [13] and $\beta = 1/(1-\sqrt{1-\varepsilon})$ [11].

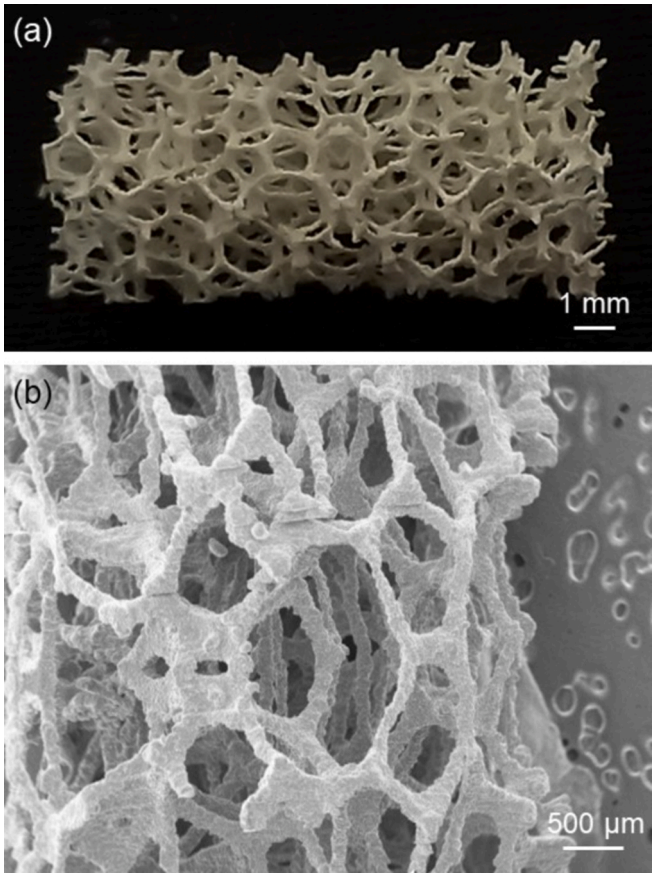

Fig. 1. BG-1d scaffolds investigated in this work: (a) macrophotograph and (b) detail of the microstructure (SEM image).

It was demonstrated that, for laminar flows (i.e., when U is low enough), the inertial losses due to the resistive term (Equation (3)) are negligible [14]. This condition is satisfied if the interstitial Reynold's number $\mathrm{Re}_i = \frac{\rho D_{av}\varphi U}{\mu(1-\varepsilon)} < 10$ (or friction factor $f_c = 72\tau\mathrm{Re}_i^{-1} + 0.75\tau > 10$), thereby assuring that the deviation from the linear condition caused by the resistive term is < 10 %. Under this assumption, the intrinsic Darcian permeability (k_D), expressed as a function of viscous losses only (Darcy' region) within the scaffold (Equation (2)), can be calculated as:

$$\frac{1}{k} = \frac{\mu a U + \rho b U^2}{\mu U} = a + \frac{\rho b U}{\mu} \Longrightarrow \frac{1}{k_D} \cong a \tag{4}$$

2.3. Experimental methods, data processing and statistics

The experimental approach followed in this work relies on the accurate determination of (i) the intrinsic Darcian permeability k_D of the scaffold by using a calibrated acoustic permeameter, and (ii) the average pore diameter D_{av} and the sphericity φ by using X-ray micro-computed tomography (micro-CT); details of the CT equipment and set-up can be found in [10].

The parameter k_D is measured by using an acoustic calibrated permeameter following a procedure described in [15]; the principle of the method relies on determining the pressure wave drop of a very slow oscillating airflow through the scaffold by means of a low-pressure field microphone.

Results are calculated from 3 repeated measurements on 7 different samples in order to take into account both the repeatability of measurements and the reproducibility of samples; further details can be found in [7]. Experimental data are subjected to a detailed uncertainty analysis according to GUM [16] and supported by a robust statistical approach: the overall uncertainties are propagated to define, with a confidence level of 95 %, the assessment of the actual microstructural parameters and mass transport properties of the scaffold.

With regard to data elaboration, Equation (2) can be rearranged so that the only unknown term is the effective porosity ε, which can be determined by calculating the zero-value(s) of the following Equation (5) in the range $0 < \varepsilon < 1$:

$$\frac{72k_D}{D_{av}^2\varphi^2} = \frac{\varepsilon^3}{(1-\varepsilon)^2}\bullet\frac{1}{1-0.4\ln(\varepsilon)} \tag{5}$$

More properly, the left (known) term of Equation (5) is expressed by propagating the experimental and statistical uncertainties of the constitutive parameters in this form: $[k_D \pm U(k_D)]$, $[D_{av} \pm U(D_{av})]^2$, and $[\varphi \pm U(\varphi)]^2$, where $U(k_D)$, $U(D_{av})$, and $U(\varphi)$ are the overall expanded uncertainties of k_D, D_{av} and φ, respectively, according to the general rule of error random propagation in GUM.

3. Results and discussion

A graphical representation of permeability data is plotted in Fig. 2 along with the results of uncertainty analysis, yielding $k_D = (4.27 \pm 1.78) \times 10^{-9}$ m^2. This result doubles the permeability of "conventional" foam-replicated 45S5 glass scaffolds (1.96×10^{-9} m^2) having 90 vol% porosity [4] (such difference is to be attributed to the higher porosity and highly-interconnected 3D-printed structure) and comparable to the values from human calcaneus ($0.4–11.0 \times 10^{-9}$ m^2) [17] and vertebral bone ($1.5–12.1 \times 10^{-9}$ m^2) [18].

Micro-CT analysis allowed assessing the average pore diameter D_{av} and pore sphericity φ. Data extraction from micro-CT returned the pore total volume V_p and surface area S_p; hence, the sphericity and average

	Intrinsic permeability $k_D \cdot 10^{-9}/m^2$	Expanded uncertainty $U(k_D) \cdot 10^{-9}$
Sample #1	4.00	0.33
Sample #2	3.91	0.59
Sample #3	4.07	0.75
Sample #4	5.03	**0.93**
Sample #5	4.02	0.39
Sample #6	5.10	0.72
Sample #7	3.78	0.60

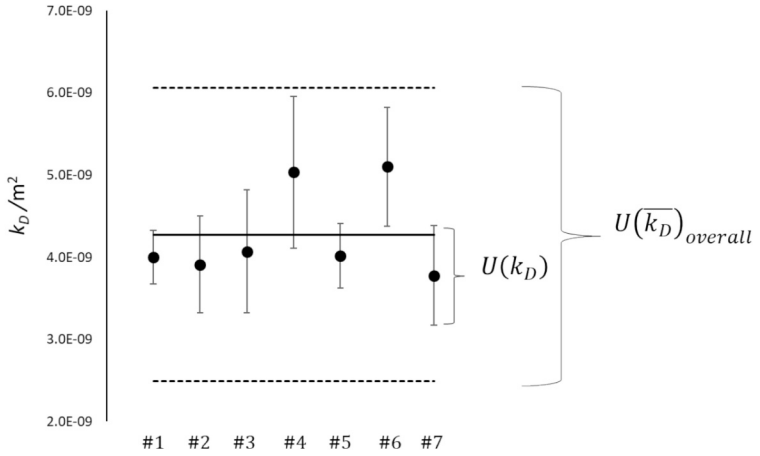

Fig. 2. Experimental data and their distribution, along with individual expanded uncertainties and the overall expanded uncertainty.

pore diameter were determined as $\varphi = \sqrt[3]{36\pi V_p^2}/S_p$ [19] and $D_{av} = 6V_p/S_p\varphi$, respectively. The total number of (open) pores analyzed was 317. Fig. 3 shows the micro-CT analysis of pores.

Due to the random distribution of pore sizes, the average pore diameter D_{av} and related standard deviation σ_n (which allows providing the relevant expanded uncertainty) were calculated on the basis of a weighted mean approach, as follows:

$$D_{av} = \frac{\sum_{i=1}^{n} D_i w_i}{\sum_{i=1}^{n} w_i} \tag{7}$$

$$\sigma_n = \sqrt{\frac{\sum_{i=1}^{n} (D_i - D_{av})^2 w_i}{\frac{n-1}{n}\sum_{i=1}^{n} w_i}} \tag{8}$$

where n is the number of the classes of the considered histogram, D_i is the central value of the pore diameter within the i^{th} class, and w_i is the weight of the mean. As the pore diameter distribution acts on pressure drop ($\partial P \propto D^{-2}$), the weight of the mean is set as the inverse of the number of occurrences included in the i^{th} class multiplied by the corresponding square diameter D_i^2, yielding $D_{av} = 1410.5 \pm 283.1$ μm. As the dataset of

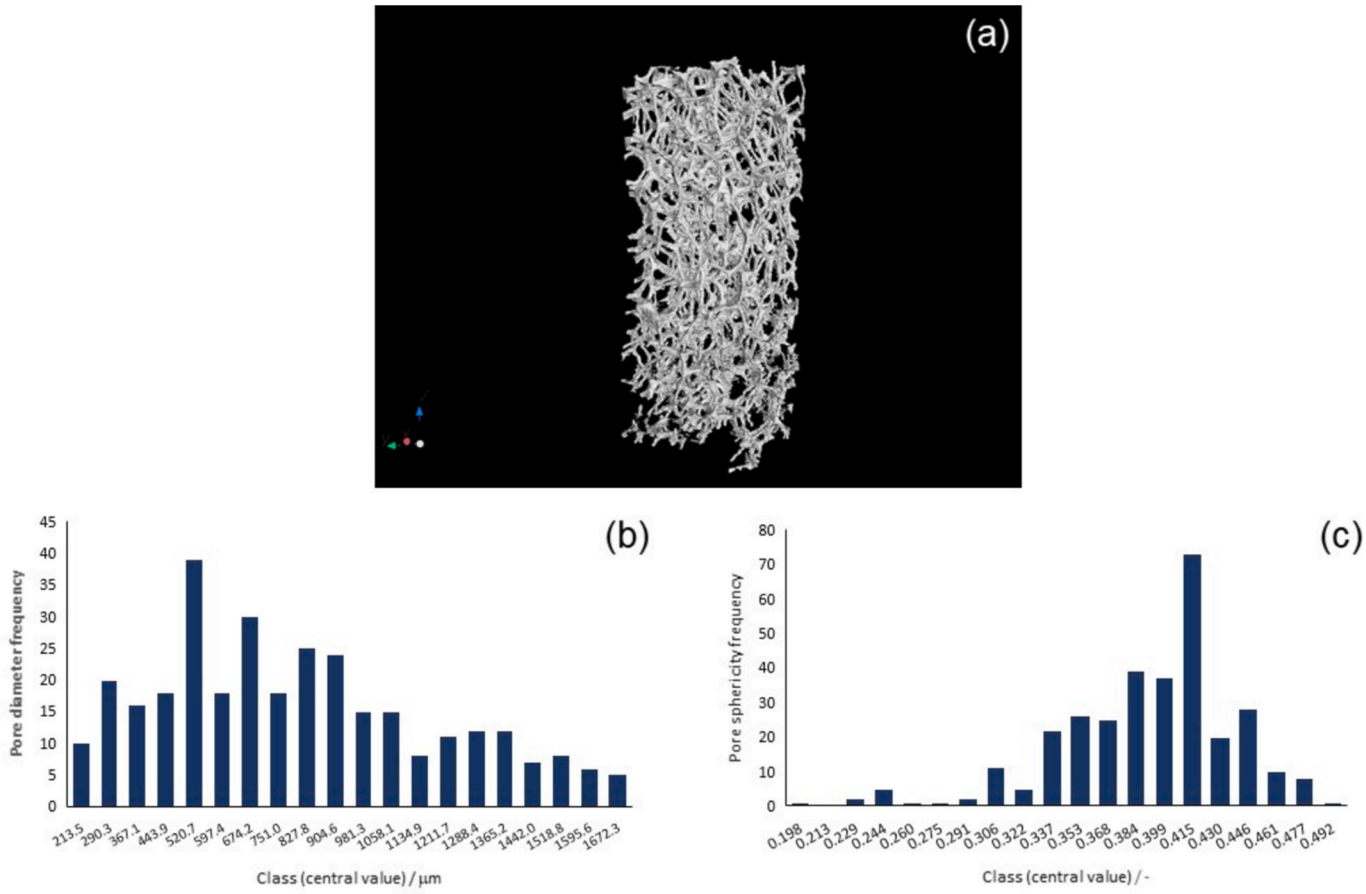

Fig. 3. Results from micro-CT analysis: (a) 3D reconstruction of the scaffold; distribution of (b) pore diameters and (c) pore shape factors.

pore shape factor followed a Gaussian-type distribution, sphericity was simply calculated in terms of arithmetic mean and standard deviation ($\varphi = 0.39 \pm 0.05$).

Once the experimental values have been determined along with related expanded uncertainties, the minimum and maximum values of effective porosity were calculated from the zero values of Equation (5); then, the ranges for microstructural parameters and mass transport properties were determined accordingly (Table 1). The tortuosity of BG-1d foams was comparable to the range calculated for radius trabecular bone by Roque et al. applying different computational approaches [20,21]. Mechanical strength of trabecular structures was reported to increase as tortuosity decreases [22], which confirms the role played by this parameter on scaffold performance. The parameter β and throat diameter D_t provide further information about transportation (e.g. physical entrapment) of cells or biomolecules throughout the pore network.

The calculated values of Re_i (<10) and f_c (>10) (Table 1) confirm the conceptual and methodological validity of the overall proposed approach.

4. Conclusions

The implementation of the Ergun-Wu model fed by experimental data (permeability: $(4.27 \pm 1.78) \times 10^{-9}$ m^2; average pore diameter: 1410 ± 283 μm) and supported by a robust statistical analysis allowed us to reliably estimate the major microstructural parameters and mass transport properties of 3D-printed ultra-porous (94 vol%) bioactive glass scaffolds. According to the results, these scaffolds show great promise for applications in contact with bone. The overall approach can be potentially applied to characterize other kinds of ultra-porous materials in a myriad of applications.

CRediT authorship contribution statement

Alessandro Schiavi: Writing – original draft, Validation, Supervision, Resources, Methodology, Investigation, Formal analysis, Data curation, Conceptualization. **Federico Gaido:** Writing – original draft, Investigation, Data curation. **Roberta Gabrieli:** Writing – original draft, Methodology, Investigation, Data curation. **Dario Alidoost:** Writing – review & editing, Investigation. **Martin Schwentenwein:** Writing – review & editing, Supervision, Methodology, Conceptualization. **Mehdi Mohammadi:** Writing – review & editing, Investigation. **Dilshat Tulyaganov:** Writing – review & editing, Methodology, Conceptualization. **Enrica Verné:** Writing – review & editing, Supervision, Resources, Methodology, Funding acquisition, Conceptualization. **Francesco Baino:** Writing – review & editing, Writing – original draft, Supervision, Resources, Project administration, Methodology, Investigation, Funding acquisition, Data curation, Conceptualization.

Declaration of competing interest

The authors declare that they have no known competing financial interests or personal relationships that could have appeared to influence the work reported in this paper.

Table 1
Summary of microstructural and mass transport properties.

Parameter	min	Max
Intrinsic Darcian permeability k_D /m^2	2.49×10^{-9}	6.05×10^{-9}
Pore diameter D_{av} /μm	1127.4	1693.6
Sphericity φ /-	0.34	0.44
Effective porosity ε /-	0.50	0.64
Tortuosity τ /-	1.18	1.28
Pore narrowing ratio β /-	2.50	3.41
Average throat diameter D_t /μm	413.1	564.2
Interstitial Reynold's number Re_i /-	1.90	5.12
Friction factor f_c /-	17.4	49.4

Acknowledgements

This study was partially carried out within the project "Artificial Intelligence-based design of 3D PRINTed scaffolds for the repair of critical-sized BONE defects - I-PRINT-MY-BONE" funded by European Union – Next Generation EU (Mission 4, Component 1, CUP: E53D23003070006) within the PRIN 2022 program (D.D. 104 - 02/02/2022 Ministero dell'Università e della Ricerca).

Data availability

Data will be made available on request.

References

[1] J.R. Jones, et al., J. Mater. Sci. Mater. Med. 20 (2009) 463–471.
[2] F.B. Wadsworth, et al., Acta Mater. 250 (2023) 118859.
[3] V. Karageorgiou, et al., Biomaterials 26 (2005) 5474–5491.
[4] I. Ochoa, et al., J. Biomech. 42 (2009) 257–260.
[5] J.R. Jones, et al., Biomaterials 28 (2007) 1404–1413.
[6] F. Baino, et al., J. Am. Ceram. Soc. 105 (2022) 1648–1657.
[7] A. Schiavi, et al., J. Eur. Ceram. Soc. 44 (2024) 4689–4698.
[8] I. Kansal, et al., Acta Biomater. 6 (2010) 4380–4388.
[9] D.U. Tulyaganov, et al., Inorganics 12 (2024) 224.
[10] F. Baino, et al., Open Ceram. 20 (2024) 100690.
[11] J. Wu, et al., Transp. Porous Med. 71 (2008) 331–334.
[12] M.T. Pamuk, et al., Exp. Thermal Fluid Sci. 38 (2012) 134–139.
[13] J. Comiti, et al., Chem. Eng. Sci. 44 (1989) 1539–1545.
[14] M.W. Chor, et al., Meas. Sci. Technol. 18 (2007) 208–216.
[15] A. Schiavi, et al., Meas. Sci. Technol. 23 (2012) 105702.
[16] JCGM 100 2008, Evaluation of Measurement Data — Guide to the Expression of Uncertainty in Measurement (GUM), France: Joint Committee for Guides in Metrology, Sèvres.
[17] M.J. Grimm, et al., J. Biomech. 30 (1997) 743–745.
[18] E.A. Nauman, et al., Ann. Biomed. Eng. 24 (1999) 517–524.
[19] H. Wadell, J. Geol. 40 (1932) 443–451.
[20] W.L. Roque, et al., Rev. Bras. Eng. Biomed. 28 (2012) 116–123.
[21] W.L. Roque, et al., IEEE Trans. Biomed. Eng. 60 (2013) 1363–1370.
[22] W.L. Roque, et al., Lect. Notes Comput. Vis. Biomech. 19 (2015) 173–191.